Our results identify a clear physiologic function for ERβ. Estrogen receptors are known to regulate a number of genes that affect vascular function (*5, 26*). Multiple ERβ-regulated gene products may contribute to the abnormal vascular contraction, ion channel dysfunction and hypertension observed in ERβKO animals. Our findings also support the concept that the transcription factor ERβ controls expression of genes critical to normal vascular physiology in both males and females. Gene targets of ERβ in relevant target tissues may provide insights into the pathophysiology and treatment of hypertension.

References and Notes

1. R. M. Evans, *Science* **240**, 889 (1988).
2. P. Walter *et al.*, *Proc. Natl. Acad. Sci. U.S.A.* **82**, 7889 (1985).
3. G. G. J. M. Kuiper, E. Enmark, M. Pelto-Huikko, S. Nilsson, J. Å. Gustafsson, *Proc. Natl. Acad. Sci. U.S.A.* **93**, 5925 (1996).
4. D. P. McDonnell, *Trends Endocrinol. Metab.* **10**, 301 (1999).
5. M. E. Mendelsohn, R. H. Karas, *N. Engl. J. Med.* **340**, 1801 (1999).
6. V. Lindner *et al.*, *Circ. Res.* **83**, 224 (1998).
7. S. Bakir *et al.*, *Circulation* **101**, 2342 (2000).
8. R. H. Karas *et al.*, *Circ. Res.* **89**, 534 (1999).
9. S. Ogawa *et al.*, *J. Hum. Genet.* **45**, 327 (2000).
10. A. P. Somlyo, A. V. Somlyo, *Nature* **372**, 231 (1994).
11. M. J. Davis, M. A. Hill, *Phys. Rev.* **79**, 387 (1999).
12. R. P. Lifton, A. G. Gharavi, D. S. Geller, *Cell* **104**, 545 (2000).
13. M. Y. Farhat, M. C. Lavigne, P. W. Ramwell, *FASEB J.* **10**, 615 (1996).
14. K. Kauser, G. M. Rubanyi, *J. Vasc. Res.* **34**, 229 (1997).
15. M. E. Mendelsohn, *Circ. Res.* **87**, 956 (2000).
16. T. Michel, O. Feron, *J. Clin. Invest.* **100**, 2146 (1997).
17. C. P. Weiner *et al.*, *Proc. Natl. Acad. Sci. U.S.A.* **91**, 5212 (1994).
18. R. L. Lantin-Hermoso *et al.*, *Am. J. Physiol. Lung Cell. Mol. Physiol.* **273**, L119 (1997).
19. J. K. Williams, M. R. Adams, D. M. Herrington, T. B. Clarkson, *J. Am. Coll. Cardiol.* **20**, 452 (1992).
20. V. Guetta *et al.*, *Circulation* **96**, 2795 (1997).
21. A. Mügge, M. Barton, H. G. Fieguth, M. Riedel, *Pharmacology* **54**, 162 (1997).
22. J. Binko, H. Majewski, *Am. J. Physiol. Heart Circ. Physiol.* **274**, H853 (1998).
23. J. H. Krege *et al.*, *Proc. Natl. Acad. Sci. U.S.A.* **95**, 15677 (1998).
24. Supplemental methods, results, figures, and references are available on *Science* Online at www.sciencemag.org/cgi/content/full/295/5554/505/DC1
25. Y. Zhu, M. E. Mendelsohn, unpublished results.
26. M. E. Mendelsohn, R. H. Karas, *Curr. Opin. Cardiol.* **9**, 619 (1994).
27. A. Y. Kolyada, N. Savikovsky, N. E. Madias, *Biochem. Biophys. Res. Commun.* **220**, 600 (1996).

28. We are grateful to N. Madias for the iNOS-luciferase reporter construct, N. Flavahan for guidance in establishing the vascular ring methods, and M. Aronovitz for superb technical assistance. Supported in part by NIH grants P50 HL63494, R01 HL55309, and R01 HL56069 (M.E.M.); NIH grant HL56235 and a Grant-in-Aid from the American Heart Association (Y.Z.); NIH grant R01 HL61298 (R.H.K.); NIH grants HD30276 and HL53546 (P.W.S.); NIH grant GM20069 (O.S.); and grants from KaroBio AB and the Swedish Cancer Fund (J-Å.G.), MFR04764 and Heart and Lung Foundation (P.T.), and from Karolinska Institute (1306/2000FFU) (Z.B.). The reported findings are solely the responsibility of the authors and do not necessarily represent the official views of the NIH.

9 August 2001; accepted 27 November 2001

REPORTS

Alternative Splicing and Neuritic mRNA Translocation Under Long-Term Neuronal Hypersensitivity

Eran Meshorer,[1] Christina Erb,[1] Roi Gazit,[2] Lev Pavlovsky,[3] Daniela Kaufer,[1]* Alon Friedman,[3] David Glick,[1] Nissim Ben-Arie,[2] Hermona Soreq[1]†

To explore neuronal mechanisms underlying long-term consequences of stress, we studied stress-induced changes in the neuritic translocation of acetylcholinesterase (AChE) splice variants. Under normal conditions, we found the synaptic AChE-S mRNA and protein in neurites. Corticosterone, anticholinesterases, and forced swim, each facilitated a rapid (minutes), yet long-lasting (weeks), shift from AChE-S to the normally rare AChE-R mRNA, promoted AChE-R mRNA translocation into neurites, and induced enzyme secretion. Weeks after stress, electrophysiological measurements in hippocampus slices displayed apparently normal evoked synaptic responses but extreme hypersensitivity to both anticholinesterases and atropine. Our findings suggest that neuronal hypersensitivity under stress involves neuritic replacement of AChE-S with AChE-R.

Traumatic stress is often followed by long-term pathological changes (*1, 2*). In humans, extreme cases of such changes are clinically recognized as posttraumatic stress disorder (PTSD) (*3*). Although the immediate response to acute stressful insults has been extensively studied, the molecular mechanisms leading to the long-term neuronal hypersensitivity that is characteristic of PTSD are yet unknown. Stimulus-induced changes in alternative splicing have recently emerged as a major mechanism of neuronal adaptation to stress, contributing to the versatility and complexity of the expression patterns of the human genome (*4–6*). Another stimulus-induced post-transcriptional process is dendritic mRNA translocation, which has been described for several transcripts (*7–12*). Because psychological, physical, and chemical stressors all cause neuronal activation and hyperexcitation, dendritic translocation of specific target mRNAs may follow.

Acetylcholinesterase (AChE) modulations provide an appropriate case study for exploring long-term stress effects. Chemical, psychological, and physical stresses all shift splicing from the primary mRNA product that encodes the synaptic membrane AChE-S multimeric protein to the normally rare "readthrough" AChE-R transcript, which yields soluble monomers (*13*). We thus examined neuronal distributions of the two splice variants, which have characteristic 3′ regions (Fig. 1A). A comprehensive search of the NCBI GenBank and EST databases revealed several AChE-S mRNAs but only a single AChE-R mRNA of rodent brain origin (GenBank accession number X70141), attesting to the scarcity and/or instability of neuronal AChE-R mRNA under normal conditions. To study changes in gene expression at the subcellular level, we used double-label fluorescence in situ hybridization (FISH) of specific AChE mRNA splice variants (*14*) and confocal microscope image analysis.

FISH detection efficiencies likely depend on probe sequences, but subcellular distributions can be reliably compared for single transcripts in different cells and conditions. Cultured PC12 cells (*15*), primary cultures of mouse cerebellar neurons (*16*), and pyramidal neurons in paraffin-embedded sections of the prefrontal cortex (*17*) all displayed a larger fraction of AChE-S mRNA transcripts in neuronal processes than of AChE-R mRNA (Fig. 1, B through D). Also, both cell types displayed nuclear localization of AChE-R but not of AChE-S mRNA (Fig. 1, B and C) (*18*). To test whether labeling properties prejudiced this conclusion, we reversed the fluorophores on the two probes (Fig. 1, B and C). In paraffin-embedded brain sections from naïve mice, cortical pyramidal neurons presented dispersed AChE-S mRNA through-

Departments of [1]Biological Chemistry and [2]Cell and Animal Biology, The Institute of Life Sciences and The Eric Roland Center for Neurodegenerative Diseases, The Hebrew University of Jerusalem, Israel 91904. [3]Departments of Physiology and Neurosurgery, Zlotowsky Center of Neuroscience, Ben Gurion University and Soroka Medical Center, Beersheva, Israel 84105.

*Present address: Department of Biological Sciences, Stanford University, Stanford, CA 94305, USA.
†To whom correspondence should be addressed. E-mail: soreq@shum.huji.ac.il

out the processes, while AChE-R mRNA was localized to the cell body. In addition, the perikaryal cytoplasm exhibited punctated concentrations of AChE-R mRNA alternating with double-labeled regions, whereas neurites had AChE-S mRNA with foci of both transcripts (Fig. 1D). The neurite contents of cultured PC12 cells and developing cerebellar neurons, also known to express ample AChE (*19*), and of prefrontal cortex neurons in vivo were 22 ± 3, 28 ± 4 and 28 ± 7%, respectively, for AChE-S mRNA but only 10 ± 2, 7 ± 2 and 11 ± 6% for AChE-R mRNA ($P < 0.05$, two-tailed Student's *t*-test). AChE-S mRNA, thus, preferentially localized in neurites (except under stress, see Fig. 1E, below).

The human *ACHE* gene includes a glucocorticoid response element (GRE) about 17 kb upstream from the transcription initiation site (Fig. 1A). In humans, a deletion adjacent to the GRE causes constitutive overexpression and anti-AChE hypersensitivity (*20*), which suggests a physiologically significant role for glucocorticoids in regulating both neuronal *ACHE* gene expression and anticholinesterase hypersensitivity. We therefore compared PC12 cells treated for 6 hours with corticosterone (10 μM, 0.1% ethanol) to control cells (0.1% ethanol). Twenty-four hours after treatment, catalytic activity against acetylthiocholine rose by 25 ± 14% ($P < 0.05$) in PC12 cells. Corticosterone, further, increased by 30 to 50% the levels of both splice variants within 24 hours ($P < 0.05$) (Fig. 2, A through H). However, the AChE-S mRNA-labeled area remained essentially unchanged under control conditions (distance from nuclear border to limit of mRNA labeling = 37 ± 13 μm) or corticosterone (34 ± 13 μm). In contrast, AChE-R mRNA labeling extended a smaller distance from the nucleus, 25 ± 9 μm under control conditions, increasing to 33 ± 17 μm under corticosterone ($P < 0.05$).

Three-hour incubation of PC12 cells with 1.5 nM EN101, an antisense oligonucleotide that induces preferential degradation of AChE-R mRNA (*15*), affected the selective, yet limited, suppression of AChE-R mRNA (30 ± 8%, $P < 0.05$), but left unchanged AChE-S mRNA levels (Fig. 2, E through H). An inversely oriented sequence, INV101, affected neither the AChE-R mRNA level nor its distribution in PC12 cells (*21*), attesting to the sequence specificity of the antisense effect. The labeled area remained unchanged either with AChE-S or AChE-R cRNA probes, following EN101 treatment, suggesting full EN101 accessibility to the cell body (Fig. 2, I and J).

To test whether EN101 is effective similarly in neurites and perikaryal subcellular sites, we employed cerebellar neurons in primary culture. DIG labeling of AChE-S mRNA was not affected differently by EN101 and INV101, in either cell body or neurites. In contrast, EN101 reduced AChE-R mRNA labeling in the cell body of cerebellar neurons in culture, down to almost 50% of its level in INV101-treated controls (*22*). This suppression was completely restricted to the perikaryon, with no difference observed for neuritic AChE-R mRNA in antisense-treated cerebellar neurons.

Cytochemical staining of catalytically active AChE (*17*) revealed intensified AChE activity in the cell bodies of corticosterone-treated cultured cerebellar neurons (Fig. 3, A and C). This suggested that the overexpressed AChE mRNA transcripts were translated to yield active enzyme. Immunocytochemical staining with an antibody targeted against recombinant AChE-S (*23*) presented apparently similar staining patterns in neurites of control and corticosterone-treated cultured cerebellar neurons (Fig. 3, B and D). This indicated that neurites under stress secrete the hormone-induced soluble AChE-R, with no increase in the synaptic membrane-associated AChE-S.

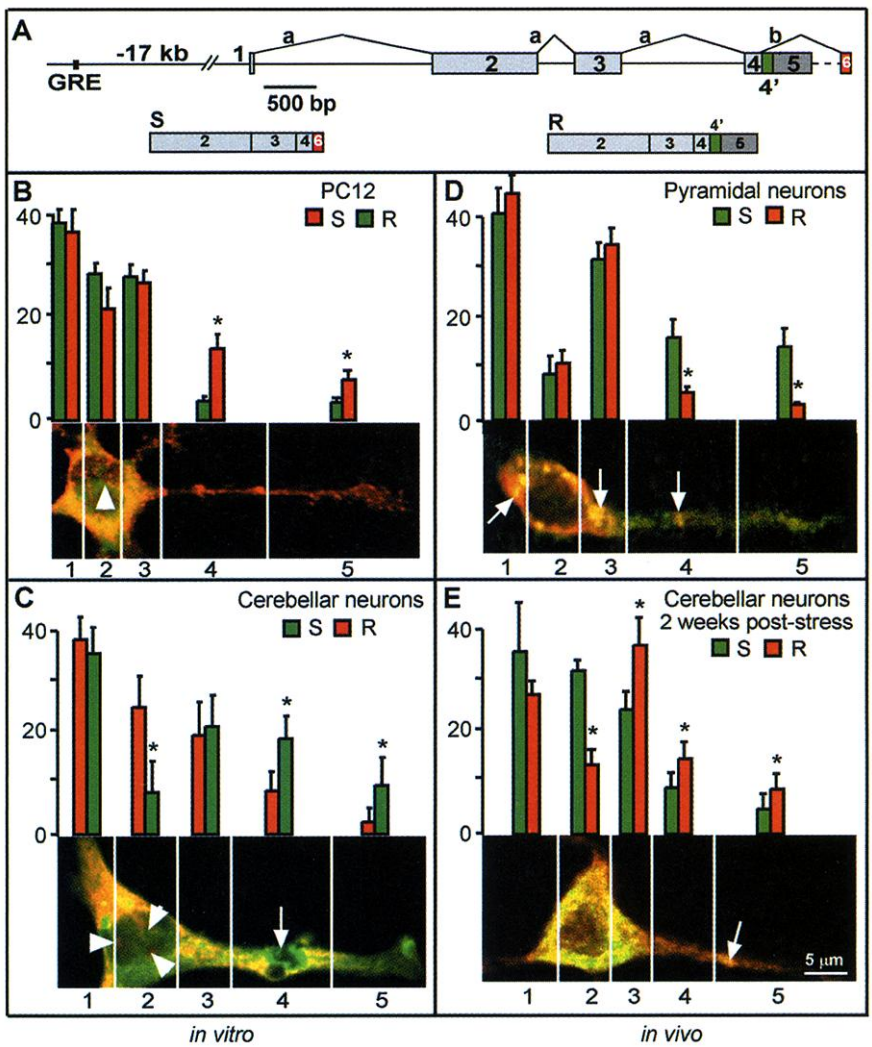

Fig. 1. Variant-specific subcellular distribution of AChE mRNAs. (**A**) Alternative splicing. Shown are the distal enhancer glucocorticoid response element (GRE) and the mouse *ACHE* gene (top), as well as AChE-S mRNA (S) and AChE-R mRNA (R). Linkage of exons 2, 3, and 4 is common to both variants (a). The R transcript includes at its 3′ terminus pseudointron 4 (green) and exon 5; option b yields the S transcript by connecting exon 4 to 6 (red). (**B** through **E**) Localization of the S and R transcripts in vitro and in vivo. Shown are percentages ± SD of FISH signals for the S and R transcripts (each totaling 100%) in three parts of the perikaryon and two neurite areas of 10 PC12 cells (B), cultured primary cerebellar neurons (C), pyramidal neurons from a paraffin-embedded slice of the prefrontal cortex (D), and cerebellar neurons from an embedded brain slice of a mouse that had been stressed for four consecutive days (2× 4 min forced swim), and sacrificed 2 weeks later (E). In control mice (D), the fraction of AChE-R mRNA in segments 4+5 was 9 ± 2% in both cortical and cerebellar neurons; for poststress mice, it was 24 ± 7% (E) ($P < 0.05$). Note nuclear labeling of the R transcript in cultured cerebellar neurons (arrowheads) and the punctated pattern of transcript accumulation in vivo [arrows in (D) and (E)]. Asterisks indicate columns with significant differences between AChE-S and AChE-R mRNAs ($P < 0.05$).

We used FISH detection of the intracellular AChE-R mRNA transcript to assess the expression levels of this variant in vivo. Dorsal hippocampus neurons of naïve FVB/N mice express extremely low levels of AChE-R mRNA under normal conditions (Fig. 3E). Two days following the stress of surgical implantation of a microdialysis cannula (*24*), the range of neurite labeling increased from 2.0 ± 0.3 to 5.1 ± 1.0 μm from the nucleus (Fig. 3G, $P < 0.0005$). Injection through the cannula of the AChE inhibitor neostigmine (125 nmol) resulted in a more extensive translocation of AChE-R mRNA within 25 min (to 8.5 ± 1.2 μm from the nucleus, Fig. 3I). In neurites of untreated hypersensitive AChE-S transgenic mice, AChE-R mRNA reached greater distances from the nucleus (9 ± 1 μm) than those of their strain-matched controls (Fig. 3F, $P < 0.0005$). Sham injection failed to further increase transport (10 ± 1 μm, Fig. 3H), but AChE-R mRNA reached dendrite distances of 15 ± 2 μm under neostigmine (Fig. 3J), significantly longer than either similarly treated nontransgenic animals, or sham injected transgenics (in both cases $P < 0.0005$; Fig. 3, K and L).

Reported rates of mRNA dendrite transport range from 10 to 20 μm·hour^{-1} (*25*) to 300 to 360 μm·hour^{-1} (*26*). In our study, assuming a constant rate, AChE-R mRNA traveled a minimum of 8 ± 5 μm·hour^{-1} in anticholinesterase-treated FVB/N mice, which increased to 14 ± 7 μm·hour^{-1} in similarly treated hAChE-S transgenic mice ($P < 0.0005$). This rate is consistent with the lower range estimate. The stability of AChE-R mRNA in the face of an antisense agent predicted long-lasting poststress neuritic presence of this transcript in vivo. To test this, we subjected FVB/N mice to 4 consecutive days of forced swim (two 4-min sessions per day). In naïve mice, cerebellar granule neuron processes were loaded with 28 ± 12% of the cellular AChE-S mRNA but only 9 ± 2% of the AChE-R mRNA content (Fig. 1C). Two weeks post-stress, a considerably larger fraction (24 ± 7%) of the stress-increased amount of AChE-R mRNA translocated into neurites and displayed patches of concentrated AChE-R mRNA in both the cell bodies and processes (Fig. 1E). Thus, both the absolute levels and the neurite fraction of AChE-R mRNA increased considerably.

In nontransgenic mice, hippocampal AChE-R mRNA is generally limited to the granular layer (*17*). AChE-R mRNA levels remained considerably higher than baseline 4 weeks after 4 consecutive days of forced swim or 3-day exposure to very low diisopropylfluorophosphonate (DFP) levels (0.1 mg·kg^{-1}·day^{-1}, i.p., LD_{50} = 2.5 mg·kg^{-1}). Prestressed or preexposed animals presented high-intensity labeling in the hippocampus CA1 region, dentate gyrus, and dendrite layer (Fig. 4, A through F), predicting modified composition of neuritic AChE variants either after stress or low-level exposure to an anticholinesterase.

Released neuronal acetylcholine binds to both pre- and postsynaptic receptors and is assumed to serve as a modulatory neurotransmitter and set the response level of the neuronal network to incoming stimuli (*27*). This involves electrophysiological mechanisms that are only partly understood, but depend on synaptic hydrolysis of acetylcholine by AChE-S. To test whether the supplementation of neuritic AChE-S with AChE-R compromises the capacity to confront intensified cholinergic stimuli, we stimulated the CA2/CA3 region of the stratum oriens, a region rich in cholinergic fibers, and recorded population field potentials (pfps), which sum the responses of a large number of neurons, in the cell body layer of the CA1 region (*17*). Recording in hippocampus slices (*28*) was performed 1 month after exposure to stress or in slices from naïve animals. The anticholinesterase physostigmine induced an increase (42 ± 15%, $P < 0.05$) in the amplitude of the evoked population spike response of naïve mice (Fig. 4, G and I). This response was 70% reversible following the addition of atropine to the bathing solution, indicating major action through muscarinic receptors. In

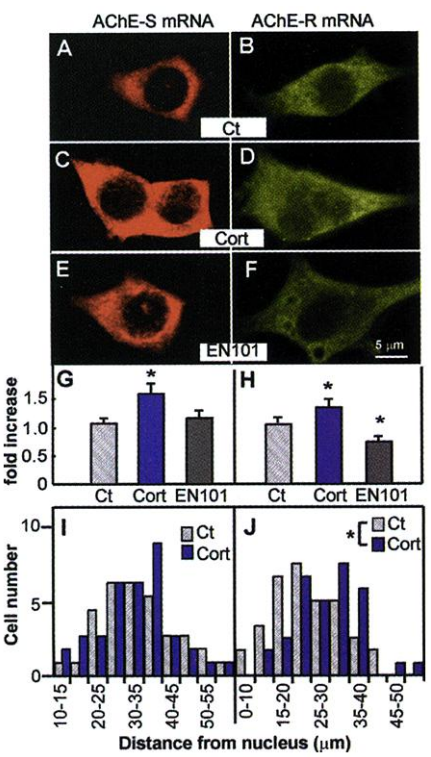

Fig. 2. Corticosterone induction and antisense suppression of AChE mRNA in PC12 cells. Shown are confocal micrographs (**A** through **F**), average labeling intensities (**G** and **H**) and distributions of distances from the nucleus to the cell border (**I** and **J**) of the S (red) and R (green) transcripts in PC12 cells (n = 40) under control conditions [(A) and (B)], or after 3 hours in 10 μM corticosterone [(C) and (D)] or 1.5 nM EN101 [(E) and (F)]. Asterisks indicate columns with significant differences from controls ($P < 0.05$). Panels (I) and (J) present the numbers of cells that contain AChE-S or AChE-R mRNA versus their maximum distance from the nucleus.

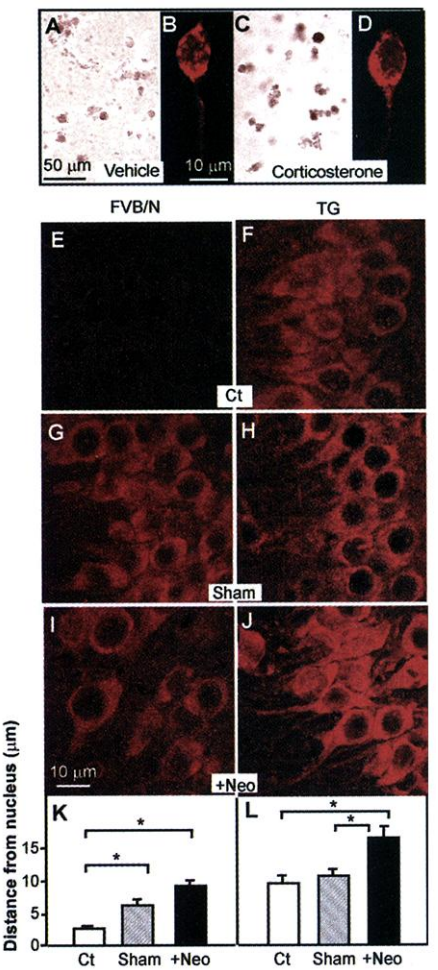

Fig. 3. Increased AChE-R expression and dendritic translocation under hormone, genetic background, sham injection, and chemical stressors. (**A** through **D**) Shown are primary cerebellar neurons stained for AChE activity under vehicle treatment [(A), 0.1% ethanol] or corticosterone [(C), 10 μM, 6 hours]. (B) and (D) Higher magnification immunocytochemical AChE-S labeling. (**E** through **J**) Confocal field images of hippocampal CA1 neurons from normal FVB/N mice [(E), (G), and (I)] and transgenic animals overexpressing human AChE [(F), (H), and (J)], under control conditions [(E) and (F)], 2 days following cannula implantation and perfusion with artificial cerebrospinal fluid [(G) and (H)], or following injection through this probe of 125 nmol neostigmine [(I) and (J)]. (**K** and **L**) Neuritic translocation of detectable AChE-R mRNA labeling (in μm from nucleus) for 30 neurons from at least two animals in each group. Significant differences from noted values are starred ($P < 0.0005$).

nonstimulated slices from animals tested 1 month following 4 days of repeated stress, the mean pfp amplitude was similar to that of nonstimulated controls. However, exposure of slices from stressed mice to physostigmine resulted in a 12-fold larger increase over baseline in stimulation-evoked population spike amplitudes than that observed in nonstressed animals. Atropine administration reversibly blocked this response by more than 90%, much more effectively than its capacity to block field potentials in the control brain (Fig. 4H versus 4G). The stronger responses to both stimulators and antagonists following stress spanned the entire range of stimulus intensity (Fig. 4, I and J), similar to the hypersensitivity patterns seen in humans as PTSD. As in control mice, the evoked pfp was blocked by the NMDA and AMPA antagonists, aminophosphonopentanoic acid (APV) and dinitroquinoxalinedione (DNQX), respectively, attesting to the glutamatergic, i.e., excitatory, nature of the hypersensitized synapses. Neuronal hypersensitivity has long been known to follow stressful experiences (*29*), but the mechanisms leading to it remained unknown. Our current findings suggest a role for stimulus-induced AChE-R overexpression and neuritic translocation in this phenomenon.

Translocation into neuronal processes presumably depends on *cis*-acting elements and/or secondary structures, primarily within the 3′ untranslated region (*26, 30*). AChE-R mRNA includes no known neurite-targeting motif; its transport into dendrites may thus be associated with its unique 3′ sequence, or with the stress-induced accumulation of many more nascent AChE-R mRNA transcripts. The normally short half-life of AChE-R mRNA, ~4 hours (*31*), also appears to be modified following stress. AChE-R mRNA includes a long U-rich element in the 3′-UTR (positions 13,020 through 13,007 in GenBank accession number AF312033), which may contribute to mRNA destabilization through the binding of *trans*-acting proteins (*32*). Although the importance of this element to the stability of AChE-R mRNA remains to be tested, the differential resistance of neurite AChE-R mRNA to antisense oligonucleotide-mediated degradation may reflect low nuclease levels in neurites, especially of ribonuclease H, which targets DNA-RNA hybrids. AChE mRNA had been shown to be stabilized during neuronal differentiation (*33*); our observations suggest that this may be due, at least partially, to AChE-R transcripts being sequestered in neurites.

The weeks-long hypersensitivity of prestressed hippocampus to anticholinesterases attributes a role to the hippocampus in the cholinergic component of post-stress sensitization. The recorded field potentials were sensitive to both cholinergic and glutamatergic antagonists, suggesting a long-term change in the interactions between these two transmitter systems. Cholinergic-glutamatergic interactions have been associated with higher brain functions such as long-term potentiation, memory, and behavior (*34*), all of which are affected by stress. The hypersensitization may also reflect an involvement of neuritic AChE-R in plasticity, due to its capacity to affect cell-cell and cell-matrix interactions (*13*).

In conclusion, we find that the stress-induced increases in cholinergic neurotransmission (*35*) promote a long-term replacement of synaptic membrane AChE-S protein by its soluble AChE-R counterpart. The long-

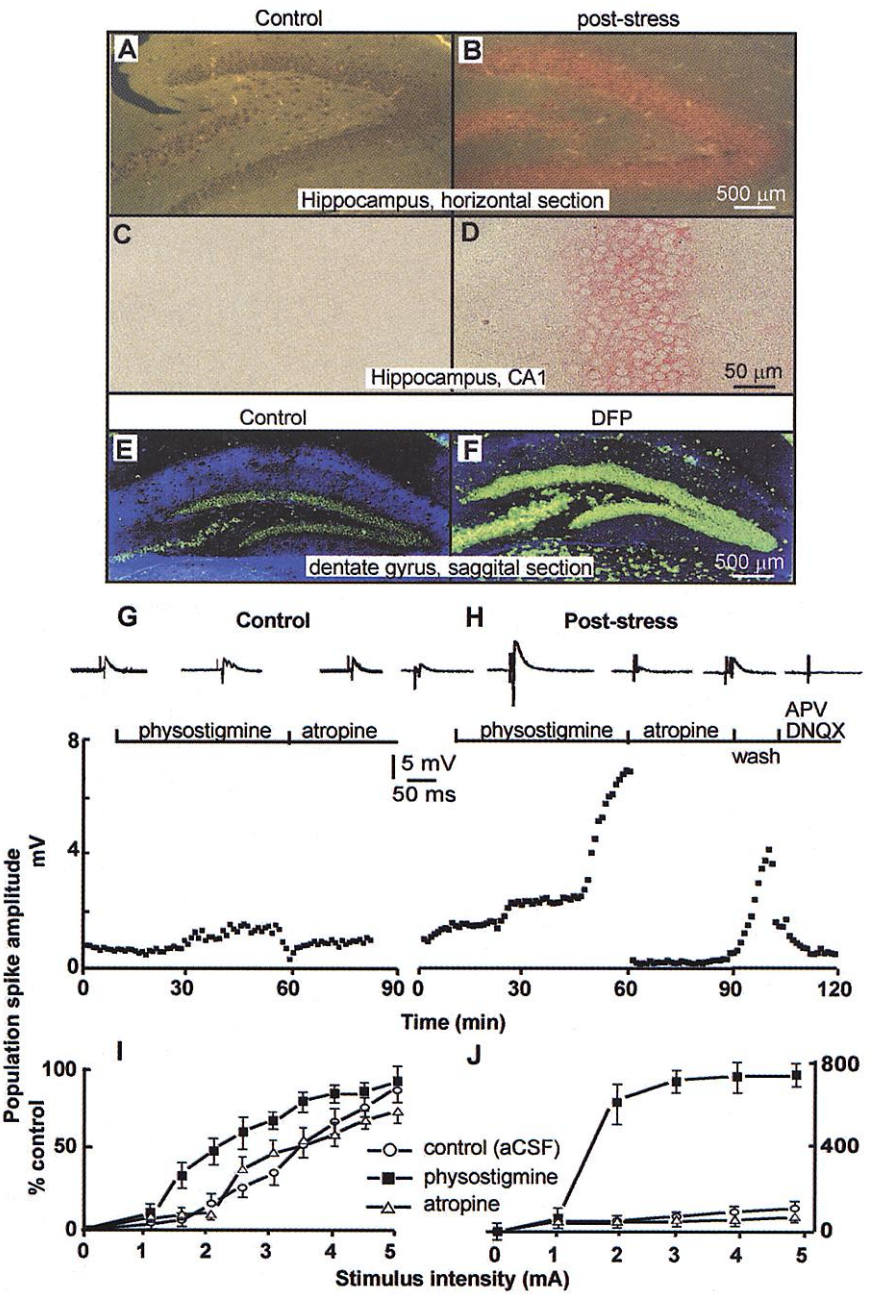

Fig. 4. Hypersensitivity in hippocampal slices under long-lasting overexpression of AChE-R mRNA. (**A** through **F**) Neuronal overexpression. Shown is a comparison of hippocampal slices from control mice to those stressed 1 month earlier by forced swim [(A) to (D), Fast Red colorimetry] or exposure to DFP [0.1 mg kg^{-1}, three consecutive daily injections, (E) and (F), ELF fluorimetry]. (**G** through **J**) Cholinergic hypersensitivity. Shown are extracellular recordings (average ± SD) on the CA1 areas of two to four hippocampus slices from each of three mice, in response to stratum oriens stimulation of slices from controls [(G) and (I)] or 1 month following consecutive daily stress sessions [(H) and (J)]. Above treatment descriptions are shown representative voltage traces. Stimulations (20 s each) were delivered using a bipolar electrode (10 μm insulated tungsten wires, 200 μm apart) placed in the Schaffer collaterals. Applied drug concentrations were: physostigmine, 10 μM; atropine, 10 μM; APV, 50 μM; DNQX, 20 μM.

term hypersensitization to repeated stimuli shown by cholinergic brain tracts may be due to this substitution.

References and Notes

1. B. S. McEwen, *Annu. Rev. Neurosci.* **22**, 105 (1999).
2. R. M. Sapolsky, L. M. Romero, A. U. Munck, *Endocr. Rev.* **21**, 55 (2000).
3. G. Mezey, I. Robbins, *Brit. Med. J.* **323**, 56 (2001).
4. J. A. McCormick *et al.*, *Mol. Endocrinol.* **14**, 506 (2000).
5. J. Xie, D. P. McCobb, *Science* **280**, 443 (1998).
6. R. Daoud, M. Da Penha Berzaghi, F. Siedler, M. Hubener, S. Stamm, *Eur. J. Neurosci.* **11**, 788 (1999).
7. L. Davis, G. A. Banker, O. Steward, *Nature* **330**, 477 (1987).
8. J. A. Foster, I. R. Brown, *J. Neurosci. Res.* **46**, 652 (1996).
9. O. Steward, C. S. Wallace, G. L. Lyford, P. F. Worley, *Neuron* **21**, 741 (1998).
10. H. Kang, E. M. Schuman, *Science* **273**, 1402 (1996).
11. C. H. Bailey, D. Bartsch, E. R. Kandel, *Proc. Natl. Acad. Sci. U.S.A.* **93**, 13445 (1996).
12. O. Steward, E. M. Schuman, *Annu. Rev. Neurosci.* **24**, 299 (2001).
13. H. Soreq, S. Seidman, *Nature Rev. Neurosci.* **2**, 294 (2001).
14. Poly-L-ornithine–coated cover slips [0.5 mg ml^{-1}, 10 min at room temperature (RT)] were sterilized by ultraviolet irradiation (TUV/c 8 W, 3 hours at RT). Cover slip–grown cells were fixed in 3% paraformaldehyde (20 min), dried (1 hour at 37°C), washed 2× 5 min in phosphate-buffered saline (PBS) and 2× 5 min in 0.2% Tween-20 PBS (PBT), incubated with 10 mg/ml proteinase K (5 min at RT), and rewashed (PBT, 2× 5 min). Streptavidin (1 mg ml^{-1}, 30 min at RT) served to block nonspecific labeling. Hybridization was in a humidified chamber with 10 μg ml^{-1} probe in 50% formamide, 5× SSC, 10 mg ml^{-1} tRNA, 10 mg ml^{-1} heparin (90 min at 52°C). Washes were in 50% formamide, 5× SSC, and 0.5% sodium dodecyl sulfate, and in 50% formamide, 2× SSC at 60°C, then at RT in tris-buffered saline (pH 7.5), with 0.1% Tween-20 (TBST) including 2 mM levamisole. Following blockade in 1% skim milk (30 min), digoxigenin-labeled probes were detected with fluorescein- or rhodamine-labeled anti-DIG antibodies (1 hour at RT, three washes in TBST). Biotin-labeled probes were detected (a) fluorometrically by conjugation with streptavidin-Cy2 or -Cy3 (Figs. 1 and 2) or (b) the ELF method (Molecular Probes, Eugene, OR) (Fig. 4, E and F), or (c) colorimetrically with streptavidin-alkaline phosphatase conjugates using Fast Red (Roche Diagnostics, Mannheim, Germany) (Fig. 3, E to J, and Fig. 4, A to D). Mounting was with Immu-Mount (Shandon, Pittsburgh, PA).
15. N. Galyam *et al.*, *Antisense Nucleic Acid Drug Dev.* **11**, 51 (2001).
16. M. Schramm, S. Eimerl, E. Costa, *Proc. Natl. Acad. Sci. U.S.A.* **87**, 1193 (1990).
17. D. Kaufer, A. Friedman, S. Seidman, H. Soreq, *Nature* **393**, 373 (1998).
18. Following hybridization with an AChE-R cRNA probe, 43 of 50 PC12 cells and 45 of 50 cultured primary cerebellar neurons displayed nuclear as well as cytoplasmic labeling. In contrast, only 9 of 50 PC12 cells and 5 of 50 primary neurons labeled for AChE-S mRNA showed nuclear labeling, reflecting different ratios of nuclear pre-mRNA to mature variant transcripts.
19. H. Soreq, D. Zevin-Sonkin, N. Razon, *EMBO J.* **3**, 1371 (1984).
20. M. Shapira *et al.*, *Hum. Mol. Genet.* **9**, 1273 (2000).
21. When treated with 1.5 nM INV101, an oligonucleotide of sequence inverse to EN101, both PC12 cells and cultured primary cerebellar neurons were labeled as extensively as untreated cells with both AChE-S and AChE-R cRNAs (n = 20 cells; SD < 17 and 12%, respectively, and $P > 0.5$ for the two probes).
22. Supplementary material is available at www.sciencemag.org/cgi/content/full/295/5554/508/DC1
23. Samples were incubated with monoclonal anti-AChE-S antibodies (Transduction Laboratories, San Diego, CA), dilution 1:200, 1 hour at RT overnight 4°C, then similar incubations with HRP-tagged goat anti-mouse secondary antibodies (1:500). Detection was with Tyramide Signal Amplification system and Cy5 fluorophore (NEN Life Science Products, Boston, MA).
24. C. Erb *et al.*, *J. Neurochem.* **77**, 638 (2001).
25. L. Davis, B. Burger, G. A. Banker, O. Steward, *J. Neurosci.* **10**, 3056 (1990).
26. C. S. Wallace, G. L. Lyford, P. F. Worley, O. Steward, *J. Neurosci.* **18**, 26 (1998).
27. R. Gray, A. S. Rajan, K. A. Radcliffe, M. Yakehiro, J. A. Dani, *Nature* **383**, 713 (1996).
28. A. Friedman, D. Kaufer, L. Pavlovsky, H. Soreq, *J. Physiol. Paris* **92**, 329 (1998).
29. S. M. Antelman, A. J. Eichler, C. A. Black, D. Kocan, *Science* **207**, 329 (1980).
30. A. Blichenberg *et al.*, *J. Neurosci.* **19**, 8818 (1999).
31. R. Y. Chan, F. A. Adatia, A. M. Krupa, B. J. Jasmin, *J. Biol. Chem.* **273**, 9727 (1998).
32. J. Guhaniyogi, G. Brewer, *Gene* **265**, 11 (2001).
33. Z. D. Luo *et al.*, *Mol. Pharmacol.* **56**, 886 (1999).
34. T. G. Aigner, *Curr. Opin. Neurobiol.* **5**, 155 (1995).
35. A. Imperato, S. Puglisi-Allegra, P. Casolini, L. Angelucci, *Brain Res.* **538**, 111 (1991).

36. We thank K. Löffleholz and J. Klein (Mainz) for fruitful discussions and N. Melamed-Book (Jerusalem) for assistance. Supported by the U.S. Army Medical Research and Materiel Command (DAMD 17-99-1-9547 to H.S. and A.F.), U.S.-Israel Binational Science Foundation (1999/115 to H.S., 1998/066 to N.B.-A., 1997/00174 to A.F.), European Community (QLG3-CT-2000-00072 to N.B.-A), and Ester Neuroscience, Ltd. (to H.S.). C.E. was a Minerva Foundation postdoctoral fellow.

2 October 2001; accepted 30 November 2001

Dynamics and Constancy in Cortical Spatiotemporal Patterns of Orientation Processing

Dahlia Sharon* and Amiram Grinvald

How does the high selectivity to stimulus orientation emerge in the visual cortex? Thalamic feedforward-dominated models of orientation selectivity predict constant selectivity during the visual response, whereas intracortical recurrent models predict dynamic improvement in selectivity. We imaged the cat visual cortex with voltage-sensitive dyes to measure orientation-tuning dynamics of a large neuronal population. Tuning-curve width did not narrow after response onset, whereas the difference between preferred and orthogonal responses (modulation depth) first increased, then declined. We identified a suppression of the evoked responses, referred to as the evoked deceleration-acceleration (DA) notch, which was larger for the orthogonal response. Furthermore, peak selectivity of the tuning curves was contemporaneous with the evoked DA notch. These findings suggest that in the cat brain, sustained visual cortical processing does not narrow orientation tuning; rather, intracortical interactions may amplify modulation depth and suppress the orthogonal response relatively more than the preferred. Thus, feedforward models and recurrent models of orientation selectivity must be combined.

Visual cortical neurons are highly selective for the orientation of stimuli presented within their receptive field (*1*), a property not shared by their thalamic inputs (*2*). How orientation selectivity arises in the cortex is still debated. Previous experiments (*3–10*) have suggested mechanisms that include feedforward (thalamically dominated) (*1*, *11*) and recurrent (intracortically dominated) (*12–15*) models. The input impinging on orientation-selective neurons has constant selectivity in feedforward models, whereas recurrent models predict improvement in selectivity during the visual response. Although single-unit methodologies excel at determining the properties of individual neurons, these properties are highly variable, making it extraordinarily difficult to obtain large samples on which to base estimates of neuronal population behavior. In optical imaging with voltage-sensitive dyes (*16*), the recorded signal accurately represents membrane-potential changes at the neuronal population level (*17*, *18*), emphasizing synaptic potentials in the dendritic tufts of cortical neurons from superficial and deep layers. Recently, this method has been improved substantially, enabling in vivo imaging of cortical neuronal population activity with millisecond temporal resolution and spatial resolution of 50 to 100 μm (*19*). We therefore used optical imaging to explore the dynamics of orientation selectivity (*9*, *20–22*).

We imaged the responses of area 18 in the cat visual cortex to high-contrast square-wave gratings of six different orientations (*23*). We examined the recording period starting 50 ms before stimulus onset and lasting 300 ms (thus avoiding late intrinsic signal

Department of Neurobiology and the Center for Studies of Higher Brain Functions, Weizmann Institute of Science, Rehovot 76100, Israel.

*To whom correspondence should be addressed. E-mail: dahlia.sharon@weizmann.ac.il